ASCE-ASME Journal of Risk and Uncertainty in Engineering Systems Part B: Mechanical Engineering
Online journal at:
asmedigitalcollection.asme.org/risk

Improving Output Power of a Torsional-Flutter Harvester in Stochastic Thunderstorms by Duffing—Van Der Pol Restoring Torque[1]

Luca Caracoglia[2]
Visiting Professor
Department of Civil, Environmental & Mechanical Engineering (DICAM),
University of Trento,
via Mesiano 77,
Trento 38123, Italy
e-mail: lucac@coe.neu.edu

Wind energy harvesters are usually designed to operate in the low wind speed range. They rely on smaller swept areas, as a complement to larger horizontal-axis wind turbines. A torsional-flutter-based apparatus is investigated herein to extract wind energy. A nonlinear hybrid restoring toque mechanism, installed at equally spaced supports, is used to produce energy through limit-cycle vibration. Energy conversion and storage from the wind flow are enabled by eddy currents. The apparatus is used during thunderstorm outflows to explore its efficiency in nonideal wind conditions. The thunderstorm flow model accounts for both nonstationary turbulence and slowly varying mean wind speed, replicating thunderstorm's intensification and decay stages. This paper evolves from a recent study to examine stochastic stability. More specifically, the output power is derived as a random process that is found numerically. Various thunderstorm features and variable apparatus configurations are evaluated. Numerical investigations confirm the detrimental effect of nonideal, thunderstorms on harvester performance with, on average, an adverse increment of operational speed (about +30%). Besides nonlinear damping, the "benign" flutter-prone effect is controlled by the square value of the flapping angle. Since flapping amplitudes are moderate at sustained flutter, activation of the apparatus is delayed and exacerbated by the nonstationary outflow and aeroelastic load features. Finally, efficiency is carefully investigated by quantification of output power and "quality factor."
[DOI: 10.1115/1.4065532]

Keywords: aeroelastic harvester, torsional flutter, thunderstorm outflows, non-stationary turbulence, stochastic differential equations

1 Introduction

Wind energy technologies are important because of the need for green energy sources. "Specialized" harvesters [1] have been proposed to exploit wind energy in the low wind speed range and for small-scale applications. These harvesters are triggered by aeroelastic instability in the airflow [2,3]. Similar devices have been considered, either triggered by water axial-flow instabilities [4], or by flutter of an inverted and flexible flag [5], or by vortex-induced vibration of cylinders inside ventilation ducts [6,7]. Recently, the exploitation of parametric excitation originating from airflow oscillation has been suggested to enhance the performance of plunge-pitch harvesters [8]. Most above-cited harvesters are, however, conceived as micromechanical units, i.e., used for recharging various types of miniature sensors.

By contrast, the field of "meso-scale" harvesting technologies has been much less explored. For example, sustained vortex-induced vibration of multi-unit circular cylinders in water flows [9] has been exploited. Recently, a hybrid device, installed on highway bridges, which can simultaneously scavenge electrical power from two different energy sources (natural wind flow and traffic-induced bridge vibrations), has been designed [10].

Along this line of research, a torsional-flutter-based apparatus has been proposed by the author [11]; the operational mechanism was inspired by seminal work by Ahmadi and coworkers [12,13]. The apparatus is composed of a nondeformable "blade-airfoil" that rotates about a pivot axis and is partially restrained through a nonlinear torsional spring mechanism, installed at equally spaced supports. Various configurations can be considered with adjustable position of the blade-airfoil pivot axis: from the leading edge (windward point) to a point closer to the quarter-chord axis position.

[1]The paper was presented at the International Mechanical Engineering Congress & Exposition® In-Person Event, New Orleans Ernest N. Morial Convention Center, October 29–November 2, 2023. IMECE2023.
[2]Permanent address: Department of Civil & Environmental Engineering, Northeastern University, 360 Huntington Avenue, Boston, MA 02115.
Manuscript received February 21, 2024; final manuscript received May 7, 2024; published online July 26, 2024. Assoc. Editor: Ioannis A. Kougioumtzoglou.

Dimensions of the harvester's blade are half-chord length and longitudinal (transverse) length. A nonlinear Duffing model and torsional spring mechanism have been used to produce limit cycle, postcritical vibration. Conversion to electrical power is warranted by an eddy current power system with multiloop magnetic coil and a translating permanent magnet [14]. Energy could be stored in a battery.

Recent studies have examined the stochastic stability of the harvester and its post-critical operational conditions in turbulent wind flows, composed of horizontal mean speed and along-wind turbulence. Nonsynoptic, nonstationary turbulence has also been considered to simulate nonideal wind flows, i.e., a gust front originating from a thunderstorm downburst [15–17], recently recorded in urban settings, where the apparatus is planned to be installed.

In this study, a recently proposed, new model is utilized to examine the mean-square stability limits. The model replaces the Duffing [18] restoring torque mechanism, used in the past [11,19], with a hybrid Duffing–van-der-Pol torque mechanism. The mechanical torque mechanism is based on standard approaches that trigger limit-cycle vibration [18] under steady, nonturbulent wind flow. The model couples the cubic-polynomial nonlinear torsional (i.e., spring-type) mechanism that opposes the self-induced torsional flapping vibration with a quadratic, amplitude-dependent equivalent damping effect and device.

Duffing–van der Pol harvesting technology has been explored to enhance micromechanical devices, triggered either by external parametric (periodic) excitation [20,21] or by stochastic sources [22]. Nevertheless, this technology has not been applied to the type of harvesters envisioned by this study. Therefore, it represents a novelty in the field of medium-size harvesters.

The main objectives of the paper are to:

(1) Reproduce the blade-airfoil aerodynamics by assuming a fully coherent thunderstorm gust front [19];
(2) investigate mean-square, stochastic stability by moment Lyapunov exponents (MLE) [23], computed numerically [24]; and
(3) expand the preliminary results, presented in a recent study [25], to analyze output power in a stochastic, non-stationary load environment.

The nomenclature table is provided in the Nomenclature section.

2 Description of the Apparatus

The apparatus (Fig. 1) is composed of a rigid blade-airfoil of dimensions b (half-chord width) and ℓ (span-wise, longitudinal length), which rotates about pivot "O." The α flapping of the rigid blade-airfoil is enabled through appropriate connection, either at equally spaced points or continuously along the span-wise direction ℓ, to a structural support (a mast in Fig. 1). The orientation of the blade-airfoil is on XY horizontal plane (Fig. 1).

The aeroelastic torque about pivot O is modeled by standard aeroelastic formulation for flat plates (i.e., a NACA0012 section of small thickness) and small angles of attack α. The load is also corrected for three-dimensional flow effects due to the finite airfoil span, i.e., through aspect ratio AR $= \ell/b$. The thunderstorm outflow combines a slowly varying, "mean" outflow wind speed U with along-wind nonstationary turbulence u. Other turbulence components are not included because they secondarily affect the blade-airfoil aeroelasticity. These two flow features simulate various development stages of the wind phenomenon, as described in Secs. 3.2 and 3.3. The aeroelastic load model plausibly replicates the main features of a gust front [26,27], originating from a nonsynoptic thunderstorm. Since the blade is longitudinally oriented on a vertical plane (XZ in Fig. 1), gravity is not relevant to energy conversion.

In Fig. 1 (top), a "nonlinear rotational restoring/damping mech [anism]" is indicated. This item is schematically described by a circular hollow container that encloses the unit's linear and nonlinear restoring and damping torsional mechanisms. A nonlinear

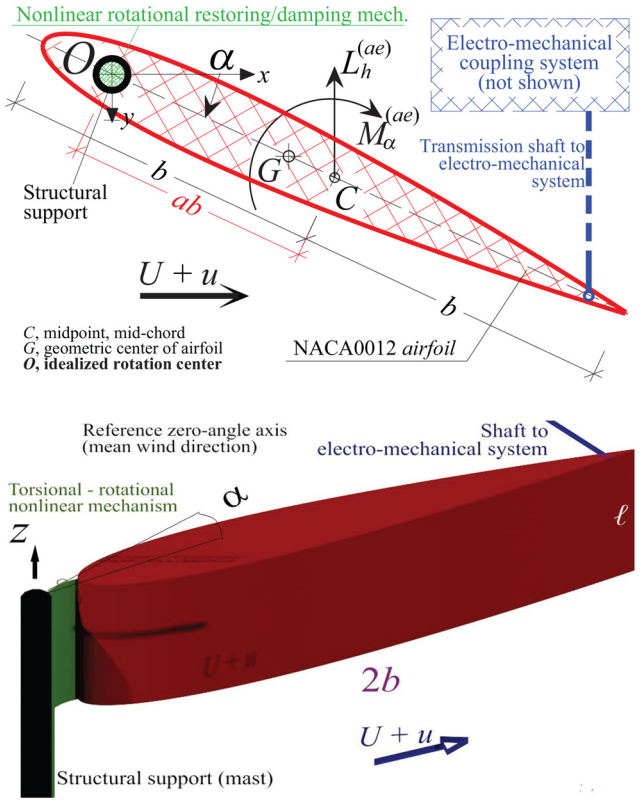

Fig. 1 Schematics of the torsional flutter harvester: (top) 2D cross-sectional view on the XY horizontal plane; (bottom) 3D rendering. Reproduced with permission from Ref. [19]. Copyright © 2024 by Elsevier.

restoring torque may be designed, for example, by embedding small, partially pretensioned loose cables inside the hollow gap; this design, at a larger scale, has been used for translating motion in nonlinear energy sinks [28] and could possibly be exploited for the flapping rotation. In the case of van der Pol energy absorption mechanism, the design concept may be borrowed from [29], who considered a vibration damper applied to a rotor; this device could possibly transform the rotor's whirling motion into a periodic "one-line" nonconservative motion [29]. Nevertheless, these design concepts are only preliminary; they will require careful consideration prior to any physical implementation. Finalized design will possibly be considered in future studies.

3 Non-Stationary Flow Fields

3.1 State-of-the-Art Review. A thunderstorm downburst is a meteorological wind phenomenon, observed during thunderstorms. The downburst is a strong downdraft flow that induces an outburst of high wind speed flows near the ground [30]. Aircraft accidents near the ground, upon landing in thunderstorms, provided the initial motivation for examining downbursts [31]. Downbursts were first recorded during thunderstorms by Doppler radar stations during the Northern Illinois Meteorological Research in Downbursts (NIMROD, 1978) and the Joint Airport Weather Studies (JAWS, 1982) projects in the USA [30,31]. Observations by meteorologists led to the derivation of methods to classify downbursts and to understand their generation mechanism [32–34]. Experimental evidence continued over time until recently, where several observations of downburst and thunderstorm outflows were reported [15,35–37] and led to a critical review of the models for fluid-structure interaction analysis in nonstationary wind flows [38,39].

Downbursts are convective, short-lived, ground-based, either dry or wet and characterized by small-scale shear winds. They evolve

and land to ground at a touchdown point, subsequently diverging and decaying over a short period of time. These convective wind fields are complex and consist of several flow velocity components: radial, vertical, horizontal, and translation velocities [33,34]. The downburst field, forming during the thunderstorm, translates because of the traveling thunderstorm path. There are two types of downburst [33]: single downburst and downburst line. A single downburst is isolated with diverging winds pointing outward in all directions from the touchdown center. The latter is a downburst case where two or three outflows form on one line, often the "straight" line of the thunderstorm track.

The wind field varies rapidly in direction, magnitude, and turbulence properties. It produces transient, nonsynoptic and short-duration wind events, which can produce complex aerodynamic loads. Transient/nonstationary downburst winds can lead to dynamic vibration on vertically oriented, flexible structures. The structural response cannot be analyzed by standard analytical methods based on stationary, synoptic winds [17].

Figure 2 illustrates a typical time series of a downburst event. It reproduces the instantaneous outflow velocity magnitude of the AAFB (Andrews Air Force Base) thunderstorm outflow, measured by an anemometer at 4.9 m elevation from the ground on Aug. 1, 1983 at 2 pm Eastern daylight time [30]. The downburst velocity record traveled through a first primary peak (67 m/s wind gust) to a secondary peak (43 m/s gust) after approximately 3 min. The instantaneous direction flow varied as the primary and secondary peaks traveled through the anemometer, from NW to SE quadrants, respectively. From Fig. 2, the following features can be noted: (i) slow time-varying mean (nonturbulent velocity), and (ii) rapidly varying fluctuations (turbulence).

3.2 Slowly-Varying Wind Speed U. Aeroelastic torque is proportional to the mean flow speed U. The thunderstorm "mean" flow is time dependent as a result of thunderstorm's evolution [34]. The time-dependent mean flow speed is rewritten as $U(\tau) = U_{\max}\Pi(\tau) > 0$. The quantity $U_{\max}$ is the maximum outflow wind speed of the thunderstorm; $\tau = \omega_\alpha t$ is a dimensionless time, with t in [s] and normalized with respect to ω_α or angular frequency of the spring-supported, linear apparatus.

Although $U_{\max}$ is recorded at a specific elevation from the ground ($20 \le z_{\max} \le 80$ m [35]) and the wind profile is not uniform, the slowly-varying outflow field is considered approximately constant with height z. Moreover, mean-wind directionality (Fig. 2 bottom) is neglected. These assumptions are plausible because the apparatus' reference diagonal dimension ($\sqrt{2b\ell}$) is small compared to $z_{\max}$; furthermore, the unit is designed to be installed on a building rooftop, close to a typical $z_{\max} = 20$ m [36].

Due to the small ($\sqrt{2b\ell}$) dimension, the main transitory feature of the thunderstorm that influences the stability is the temporal intensification, $\Pi(\tau)$. If the mean flow speed is substituted by $U(\tau) = U_{\max}\Pi(\tau)$, intensification (intensity factor) is derived from [40], as explained in Ref. [19]

$$\Pi(\tau) = \begin{cases} \dfrac{\tau}{\tau_{\max}} & 0 \le \dfrac{\tau}{\tau_{\max}} \le 1 \\ e^{-0.52\left[\frac{\tau}{\tau_{\max}}-1\right]} & \dfrac{\tau}{\tau_{\max}} > 1 \end{cases} \tag{1}$$

If dimensional time t is used in Eq. (1), with $t = \tau\omega_\alpha$; $t_{\max}$ (or $\tau_{\max}$) is the time instant corresponding to maximum intensification [34,40]. Since $t_{\max}/T \approx 0.52$, using $T = 1200$ s as the total thunderstorm duration from initial touchdown to full decay [34,40] and $t_{\max} \approx 630$ s from [41], Eq. (1) is obtained. Furthermore, using typical values of ω_α from [11], $\tau_{\max}$ is found as about $400 < \tau_{\max} < 1000$ if the total duration is referred to the AAFB thunderstorm [41], or $200 < \tau_{\max} < 500$ if $t_{\max} \approx 300$ s is extrapolated from data presented by Ref. [35].

3.3 Random Turbulence Field. The along-wind turbulence component u influences the dynamic pressure and load. It is random, nonstationary, and aptly normalized. The properties of the corresponding stationary process are represented by reduced turbulence spectrum [16]. If $\hat{u}(\tau) = u(\tau)/U_{\max}$ is the dimensionless stationary turbulence, the spectrum of the stationary process is $S_{\hat{u}}(\omega)$ and, without any loss of generality, it is a Gaussian white noise process with nonzero standard deviation. The standard deviation of the stationary turbulence is $\sigma_{\hat{u}}$.

The nonstationary thunderstorm-like turbulence features are reproduced as $\hat{u}\varphi_{\mathrm{mf}}$, i.e., by multiplication with modulation φ_{mf} [15,16] so that the evolutionary turbulence spectrum is $S_{\hat{u},\mathrm{EPSD}}(\omega,\tau) = S_{\hat{u}}(\omega)\varphi^2_{\mathrm{mf}}(\tau)$ [16].

The function $0 \le \varphi_{\mathrm{mf}}(\tau) \le 1$ is deterministic [16]. $\varphi_{\mathrm{mf}}(\tau)$ is derived from the temporal modulation $A_F(t) = \alpha_0 t^{\beta_0} e^{-\lambda t}$ proposed by Chen [42], with time t in (s) units, decay λ in (s^{-1}) and dimensionless shape parameters α_0, β_0. The parameters of $A_F(t)$ are not independent; $\lambda \approx 1\,s^{-1}$ can be used [41,43]. If $\tau_{\max}$ designates the dimensionless time instant of maximum turbulence intensification (same as $\tau_{\max}$ in Eq. (1)), $A_F(t)$ is transformed into φ_{mf} [19]

$$\varphi_{\mathrm{mf}}(\tau) = e^{\left(\frac{\tau_{\max}-\tau}{\omega_\alpha}\right)}\left(\frac{\tau}{\tau_{\max}}\right)^{\tau_{\max}/\omega_\alpha} \tag{2}$$

with $\beta_0 = \lambda\tau_{\max}/\omega_\alpha$. Equation (2) is valid if $\tau_{\max} > 0$. As indicated in the previous section, $\tau_{\max} = t_{\max}\omega_\alpha$ depends on the total duration of the thunderstorm (only). Furthermore, since the diagonal dimension of the blade-airfoil ($\sqrt{2b\ell}$) is small compared to the integral turbulence length scales, the nonstationary gusty field is basically coherent across the apparatus in Fig. 1.

Finally, it is noted that stationary turbulence u is approximated by a Gaussian white noise. It would be possible to readily include a more accurate u description, e.g., by exploiting autoregressive turbulence model representation in the time domain [44,45]. For the sake of stochastic model compactness, however, the "colored-noise" representation [45] was not included in this preliminary model.

3.4 Instantaneous Dynamic Pressure. The dynamic pressure, needed to find the aeroelastic load, combines the effects of the slowly varying mean $U(\tau) = U_{\max}\Pi(\tau)$ and turbulence $u(\tau)$. The total, instantaneous dynamic pressure is equal $1/2\rho[U(\tau)+u(\tau)]^2$, i.e., proportional to the air density ρ and the squared velocity $(m/s)^2$

$$\begin{aligned}[U(\tau)+u(\tau)]^2 &\approx U^2(\tau) + 2U(\tau)u(\tau) \\ &= U^2_{\max}\Pi^2(\tau) + 2U^2_{\max}\Pi(\tau)\varphi_{\mathrm{mf}}(\tau)\hat{u}(\tau)\end{aligned} \tag{3}$$

In Eq. (3), the product $\hat{u}\varphi_{\mathrm{mf}}(\tau)$ produces the nonstationary turbulence features. In dynamics and wind engineering, it is

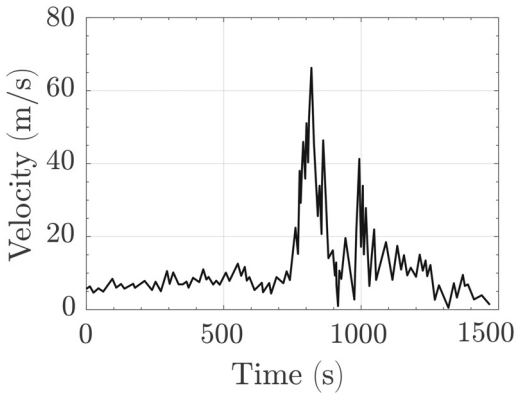

Fig. 2 Horizontal flow velocity time series of the AAFB downburst; the plot is adapted from Ref. [30]

customary to approximate the dynamic pressure by truncating the expansion to the first-order Taylor expansion (Eq. (3)). Neglecting higher order terms is acceptable since the random $\hat{u}^2(\tau)$ is proportional to the squared value of the turbulence intensity, yielding an approximation error smaller than 4% within the turbulence variations in typical atmospheric winds.

4 Dynamic Equilibrium Equation

4.1 Duffing Model. The physical states are torsional rotation α and derivative $d\alpha/d\tau$ with respect to dimensionless time τ. The dynamic equilibrium equation of the flapping rotation is [11,25]

$$\frac{d^2\alpha}{d\tau^2} + 2\zeta_\alpha \frac{d\alpha}{d\tau} + \alpha + \kappa\alpha^3 = \frac{M_{0z} + M_{(e.m.)}}{\omega_\alpha^2 I_{0\alpha}} \tag{4}$$

Nonlinear restoring force effect is simulated by the term $\kappa\alpha^3$ with κ suitable positive constant; $I_{0\alpha}$ is the total polar mass moment of inertia about pivot O. Structural damping is simulated through a linear term in Eq. (4) with damping ratio $0 < \zeta_\alpha < 1$.

The external torsional moment is about pivot O in Fig. 1. Noting the distance *ab* from the midchord point, the pivot axis position can vary between the leading edge ($a = -1$) and the one-quarter chord position ($a = -0.75$). The moment is composed of aeroelastic torque M_{0z} and electromotive torque

$$M_{(e.m.)} = -(1-a)b\Phi_{(e.m.c.)}I(\tau) \tag{5}$$

with $I(\tau)$ being the output current of the power system; $\Phi_{(e.m.c.)}$ is the electromechanical coupling coefficient in units of newton/ampère [11]. The moving coil introduces magnetic induction and interacts with a moving shaft, translating inside the winding coil (shown in Ref. [11]).

4.2 Hybrid Duffing–Van-der-Pol Model. The equilibrium incorporates both Duffing and van-der-Pol models to possibly improve energy conversion. The modified equation reads [25]

$$\frac{d^2\alpha}{d\tau^2} + 2\zeta_\alpha(1-\gamma\alpha^2)\frac{d\alpha}{d\tau} + \alpha + \kappa\alpha^3 = \frac{M_{0z} + M_{(e.m.)}}{\omega_\alpha^2 I_{0\alpha}} \tag{6}$$

In Eq. (6), besides parameter κ, a nonlinear damping effect with coefficient γ is introduced. The parameter γ models the self-limiting feature of the negative damping mechanism proportionally to the linear term $2\zeta_\alpha$.

4.3 Aeroelastic Torque

4.3.1 Stationary, Time-Dependent Loads. Mean aerodynamic forces are zero since static lift force is negligible at $\alpha \approx 0$ due to blade symmetry. In the absence of turbulence and with uniform, stationary flow, the aeroelastic torque depends on: static lift coefficient slope at $\alpha = 0$ or $\partial C_L/\partial\alpha = 2\pi$ [46], time-independent mean speed U [11] with mean direction (orientation of the blade-airfoil) parallel to the x axis in Fig. 1. Aeroelastic torque in a stationary airflow is modeled in the time domain by flow memory theory, i.e., *Wagner*'s [47] indicial function formulation [46], corrected for lift and torque reduction due to three-dimensional flow, which depends on the aspect ratio $AR = \ell/b$. The Wagner's indicial function [47] of the load is [48]

$$\Phi(\tau) = [1 - c_1 e^{-d_1 \tau k_\alpha^{-1}} - c_2 e^{-d_2 \tau k_\alpha^{-1}}] \tag{7}$$

with reduced frequency $k_\alpha = \omega_\alpha b/U$ and suitable load parameters: $c_1 = 0.165, d_1 = 0.0455, c_2 = 0.335, d_2 = 0.3$ [48] for an idealized, symmetric NACA0012 section (Fig. 1). Three-dimensional flow effects on the loads will be discussed in Sec. 5.1.

4.3.2 Non-Stationary Aeroelastic Load Perturbation. As described in Sec. 4.3.1 and in the presence of nonstationary winds, $\Phi(\tau)$ is a short temporal load evolution that is approximately independent of the gust front's instantaneous features, i.e., Eq. (1).

In a nonstationary load setting with slowly-varying mean wind speed, the reduced frequency approximately depends on U_{max}, i.e., $k_\alpha = \omega_\alpha b/U(\tau) \approx \omega_\alpha b/U_{max}$. Consequently, variability in the unsteady load can plausibly be concentrated in the parameters of $\Phi(\tau)$ and are secondarily attributed to temporal variations of U and Eq. (3).

Perturbation is introduced by replacing the deterministic parameter $d_2 = 0.3$ in Eq. (7) with a random, time dependent $d_2 = d_{2,m} + \delta_2(\tau)$; $d_{2,m} = 0.3$ and $\delta_2(\tau)$ is a zero-mean, Gaussian perturbation; $\delta_2(\tau)$ also accounts for aeroelastic load measurement error and any modeling simplifications.

The reason for exclusively considering randomness in the d_2 parameter is because the second exponential term $\{c_2 e^{-d_2 \tau k_\alpha^{-1}}\}$ primarily controls the rapidly varying load variations through Eq. (7); this term is mainly responsible for the flow memory effects.

5 Stochastic Differential Equations

5.1 Fundamental Dynamic Model Equation. If the rotation axis is at the leading edge ($a = -1$) the dynamic equation of the flapping angle is [19]

$$\begin{aligned}\left(1 + \frac{9}{8\epsilon\eta_{3D}}\right)\frac{d^2\alpha}{d\tau^2} + \left(1.5\epsilon\eta_{3D}k_\alpha^{-1} + 2\zeta_\alpha\right)\frac{d\alpha}{d\tau} \\ + \alpha + H_{NL}\left(\alpha, \frac{d\alpha}{d\tau}\right) = -\Psi\imath \\ - \frac{\epsilon\eta_{3D}}{k_\alpha^2}\Pi^2\left(1 + \frac{2\varphi_{mf}}{\Pi}\hat{u}\right)\left[\Phi_0\left(\alpha + 1.5k_\alpha\frac{d\alpha}{d\tau}\right)\right. \\ \left. + 1.5(\nu_{ae,1} + \nu_{ae,2}) + \mu_{ae,1} + \mu_{ae,2}\right]\end{aligned} \tag{8}$$

where both Π and φ_{mf} depend on time τ; $\Phi_0 = \Phi(0) = 0.5$. Quantity $\Psi = 4b^2(\Phi_{(e.m.c.)})^2/(\omega_\alpha I_{0\alpha} R_C)$ is a dimensionless electromechanical coupling coefficient of the eddy-current power circuit; R_C is the resistance of the power circuit; $\nu_{ae,1}(\tau)$, $\mu_{ae,1}(\tau)$, $\nu_{ae,2}(\tau)$ and $\mu_{ae,2}(\tau)$ are four time-dependent aeroelastic states; and $\epsilon = \pi\rho b^4 \ell (I_{0\alpha})^{-1}$ [11] is an inertia parameter. Parameter $\eta_{3D} = AR/(AR+2)$ [49] accounts for three-dimensional flow and load effects.

On the left-hand side of Eq. (8) the nonlinear function $H_{NL}(\alpha, d\alpha/d\tau)$ is used to differentiate between Duffing model (Eq. (4)) [25]

$$H_{NL} = \kappa\alpha^3 \tag{9}$$

and Hybrid Duffing–van-der-Pol one [Eq. (6)] [25]

$$H_{NL} = \kappa\alpha^3 - 2\zeta_\alpha\gamma\alpha^2\frac{d\alpha}{d\tau} \tag{10}$$

The eddy current equation of the power circuit with electromechanical coupling is found by magnetic induction [11,14]. This equation reads $d\imath/d\tau = \lambda_{RL}(d\alpha/d\tau - \imath)$, where $\imath(\tau) = I(\tau)[2b\omega_\alpha\Phi_{(e.m.c.)}/R_C]^{-1}$ is the dimensionless output current; $\lambda_{RL} = R_C/(\omega_\alpha L_C)$ is the generalized impedance (R_C resistance, L_C inductance). This equation is combined with Eqs. (8) and (9) or Eqs. (8) and (10) to form a state-space model, composed of seven nonlinear, coupled electromechanical equations. Detailed description of these equations is omitted for the sake of brevity but may be found in Refs. [19,25].

5.2 Itô-Type Differential Vector Equation. The turbulence variable $\hat{u}$ is expressed by a Gaussian process; consequently $\hat{u}$ dependency is represented by Wiener processes in the context of stochastic differential equations [50,51], Itô-type [52]. After suitable manipulations, it is found

$$\begin{aligned} d\mathbf{W}_{em} = {} & \mathbf{q}_{em,NL}(\mathbf{W}_{em})d\tau \\ & + \sqrt{2\pi}[\mathbf{t}_{NL,\hat{u}}(\mathbf{W}_{em})dB_{\hat{u}}(\tau) \\ & + \mathbf{Q}_{L,\Delta 2}\mathbf{W}_{em}dB_{\Delta 2}(\tau)] \end{aligned} \tag{11}$$

$\mathbf{W}_{em} = [\alpha, d\alpha/d\tau, \nu_{ae,1}, \nu_{ae,2}, \mu_{ae,1}, \mu_{ae,2}, \imath]^T$ in Eq. (11) is the state vector; $\mathbf{W}_{em}$ includes both physical, aeroelastic states, and dimensionless output current $\imath$.

In Eq. (11), the scalar, Wiener noise $B_{\hat{u}}(\tau)$ of unit variance increments separately addresses turbulence perturbation from the noise $B_{\Delta 2}(\tau)$, used for load perturbation. Quantity $\mathbf{q}_{em,NL}$ is a nonlinear vector-function; $\mathbf{t}_{NL,\hat{u}}$ is a nonlinear turbulence diffusion vector-function. $\mathbf{Q}_{L,\Delta 2}$ is a constant, diffusion matrix that controls the load perturbation and depends on the standard deviation of $\delta_2(\tau)$, σ_{d2}.

Both $\mathbf{q}_{em,NL}$ and $\mathbf{t}_{NL,\hat{u}}$ incorporate dependency on $\Pi(\tau)$, $\varphi_{mf}(\tau)$ and $\sigma_{\hat{u}}$. Derivation of $\mathbf{q}_{em,NL}$ is omitted for the sake of brevity but is described in Ref. [19]; $\mathbf{t}_{NL,\hat{u}}(\mathbf{W}_{em})$ is a 7×1 vector function with one nonzero element only

$$\begin{aligned} [\mathbf{t}_{NL,\hat{u}}(\mathbf{W}_{em})]_2 = {} & \frac{2\Pi\varphi_{mf}\sigma_{\hat{u}}(\epsilon\eta_{3D})^2}{(9/8+\epsilon\eta_{3D})k_\alpha^2}\Big|\Phi_0(W_{em,1} \\ & + 1.5k_\alpha W_{em,2}) + W_{em,5} + W_{em,6} \\ & + 1.5(W_{em,3} + W_{em,4})\Big| \end{aligned} \tag{12}$$

In the previous equation the symbol $|.|$ designates absolute value operator. The nonzero elements of the 7×7 $\mathbf{Q}_{L,\Delta 2}$ matrix that left-multiplies $\mathbf{W}_{em}$, are

$$[\mathbf{Q}_{L,\Delta 2}]_{4,2} = [\mathbf{Q}_{L,\Delta 2}]_{6,1} = \sigma_{d2}k_\alpha^{-1}c_2 \tag{13a}$$

$$[\mathbf{Q}_{L,\Delta 2}]_{6,6} = -\sigma_{d2}k_\alpha^{-1} \tag{13b}$$

The Wong and Zakai correction terms [53] are introduced in Eqs. (12) and (13).

Equation (11) must be solved with appropriate initial conditions, imposed on the random state vector at $\tau = 0$. Initial conditions are imposed by assuming nonzero random initial flapping, compatible with the plausible triggering mechanism, expressed as a random, Gaussian, scalar angle perturbation α_0 into the first element of the sate vector with given properties, while other states have identically zero initial values, i.e., $\mathbf{W}_{em}(0) = [\alpha_0, 0, \ldots, 0]^T$.

5.3 Mean-Square Stability. The standard asymptotic stability analysis [54] relies on the various definitions of stochastic stability, among which the use of MLE [24] is usually considered in the context of wind-excited nonlinear systems [55–58] such as the one in Eq. (11). The MLE measures the propensity of the system's slow dynamics to asymptotically exhibit a diverging oscillatory trend. It can be interpreted as a generalized measure of damping ratio in a linear system. The MLE cannot usually be found in closed form; stability must be studied numerically. Asymptotic stability entails that Eq. (11) is first solved in weak form, i.e., by numerical integration that is repeated several times through Monte Carlo sampling [24]. Second, the ensemble of the solutions is collected and utilized to examine stability. The mean-square stability requires the evaluation of the second MLE of the subvector $\boldsymbol{\Upsilon} = [\alpha, d\alpha/d\tau, \imath]^T$

$$\Lambda_{\boldsymbol{\Upsilon}}(2) \approx \frac{\log_e\left(\mathbb{E}[\|(\boldsymbol{\Upsilon}(\tau_l)\|^2]\right)}{\tau_l} \tag{14}$$

where $\mathbb{E}[.]$ is the expectation operator applied to the Euclidean vector norm; $\boldsymbol{\Upsilon}(\tau_l)$ is evaluated at time $\tau_l > 0$; time τ_l is sufficiently large, i.e., Eq. (14) approximates the limit as $\tau_l \to +\infty$ to study stability [24]. The vector $\boldsymbol{\Upsilon}$ in Eq. (14) also includes the output current $\imath$ to evaluate the effect on operational conditions and energy conversion.

Equation (14) is employed, at least approximately, to investigate environments contaminated by nonstationary, thunderstorm gusty winds, noting that the asymptotic value, defined in Eq. (14), is rather elusive and should possibly be referred to a finite time τ_l, at least greater than τ_{max} or possibly beyond the duration of the thunderstorm.

6 Stochastic, Postcritical Output Power Estimation

6.1 Input Power. The output power can be estimated as well as the efficiency, absorbed by the secondary circuit, not shown in Fig. 1 but schematically described in previous studies [11].

First, the input power is evaluated, as described in Ref. [19], in closed form by using the equivalent swept area orthogonal to the XZ plane in Fig. 1, i.e., the flow that passes through the cross-sectional area of the apparatus $[2b(2\alpha_{pk})\ell]$. If $2\alpha_{pk}$ is designated as the maximum ("pk" = peak) flapping amplitude during post-critical operations, the time-varying instantaneous wind speed cubed is $[U_{max}\Pi(\tau) + U_{max}\varphi_{mf}(\tau)\hat{u}(\tau)]^3$, where the random, zero-mean, stationary along-wind turbulence $\hat{u}$ is modulated by $\varphi_{mf}(\tau)$ (Eq. (2)) and the slowly-varying mean flow by $\Pi(\tau)$ (Eq. (1)). The input power is stochastic because of the random $\hat{u}$ and the flapping angle α_{pk} [19]

$$\begin{aligned} P_{in}(\tau) = {} & 2b\ell\rho(\alpha_{pk})U_{max}^3\Pi^3(\tau) \\ & \times\left[1 + 3\hat{u}(\tau)\frac{\varphi_{mf}(\tau)}{\Pi(\tau)}\right] \end{aligned} \tag{15}$$

The random parent process of the peak process α_{pk} is $\alpha(\tau)$, which is zero-mean, controlled by aeroelasticity, and is approximately Gaussian because of Eq. (11).

As described by Ref. [19], it is found: $\alpha_{pk} = \sigma_\alpha(\tau)g_{\alpha,T}(\tau)$; $\sigma_\alpha(\tau) = \sqrt{\mathbb{E}[\alpha^2(\tau)]}$ is the standard deviation (root-mean-square) of the zero-mean flapping angle process. Equation (15) implies that the random flapping angle has zero mean, $\mathbb{E}[\alpha(\tau)] = 0$.

Furthermore, $g_{\alpha,T}(\tau)$ in Eq. (15) is a random, peak effect factor defined over the reference, total duration of the thunderstorm T. Quantity $g_{\alpha,T}(\tau)$ is approximated by its stationary Gaussian process and assumes weak coupling between $g_{\alpha,T}(\tau)$ and $\hat{u}(\tau)$ so that the expected value of their product is zero [19]. Since $\mathbb{E}[\hat{u}(\tau)] = 0$, thus Eq. (15) is approximated as

$$\begin{aligned} \mathbb{E}[P_{in}(\tau)] &= 2b\ell\rho\mathbb{E}[\alpha_{pk}U^3(\tau)] \\ &\approx 2b\ell\rho U_{max}^3\Pi^3(\tau)\sigma_\alpha(\tau)\mathbb{E}[g_{\alpha,T}(\tau)] \end{aligned} \tag{16}$$

The expected value of the peak effect factor in Eq. (16) is found from Davenport [59]. In fact, under the assumption of weak non-stationarity, the expectation $\mathbb{E}[g_{\alpha,T}(\tau)]$ is approximately time-independent. Figure 8 in Ref. [19] shows that $\mathbb{E}[g_{\alpha,T}(\tau)]$ varies between 2.85 and 3.52 within the practical range of τ_{max} and can be evaluated by Davenport's formula for random, stationary vibrations [59]. The mean up-crossing rate of the stationary peak process α, is needed by Davenport's formula; this is conservatively estimated as the rate of zero up-crossings or $\nu_{0\alpha}^+$, plausible since $\mathbb{E}[\alpha] = 0$ and α is a narrow-band process. Furthermore, it is found through the flapping frequency of the harvester, i.e., $\nu_{0\alpha}^+ \approx \omega_\alpha/(2\pi)$ Hz, which is suitable for predominantly resonant response α. Reference [19] also notes that $\nu_{0\alpha}^+T \approx \omega_\alpha T/(2\pi) = (\tau_{max}/t_{max})T/(2\pi) \approx 1.92\tau_{max}/(2\pi)$, with $\nu_{0\alpha}^+$ being the rate of α zero up-crossings. Therefore, the expected value of $g_{\alpha,T}(\tau)$ becomes

$$\mathbb{E}[g_{\alpha,T}(\tau)] = \bar{g}_{\alpha,T} \approx \sqrt{2\log_e\left(\frac{1.92}{2\pi}\tau_{\max}\right)} + \frac{0.577}{\sqrt{2\log_e\left(\frac{1.92}{2\pi}\tau_{\max}\right)}} \tag{17}$$

Equation (17) is also acceptable since it over-estimates the actual peak effect that is largest for sustained buffeting vibration [26]. By contrast, limit-cycle post-critical flapping is usually pseudo-periodic and characterized by a $\sqrt{2}$, i.e., usually acceptable for sustained aeroelastic, vortex-induced transverse vibration [60]. Even though an extended formulation of this factor has been recently found for nonstationary thunderstorm gust effects by closed-form solution [61], a more refined estimation is unnecessary for this study's purposes but may be considered in future studies.

6.2 Output Power Coefficient. The stochastic postcritical, output power is calculated as $\mathrm{P}_{\mathrm{out}}(\tau) = R_C I^2(\tau)$ [19]. The expected value of the output power is

$$\mathbb{E}[\mathrm{P}_{\mathrm{out}}(\tau)] = \frac{\left(2b\omega_\alpha \Phi_{(\mathrm{e.m.c.})}\right)^2}{R_C}\mathbb{E}\left[\imath^2(\tau)\right] \tag{18}$$

Equation (18) implies nonstationarity and, if evaluated numerically, can also assess temporal variations of power due to the transitory dynamics of Eq. (11). Moreover, the mean-square value of the dimensionless current is used to imply that, because of nonlinearity in Eq. (8), damping "a-symmetries" (α^2 term in Eq. (10)) may possibly lead to nonzero output current. Consequently, the τ-dependent, expected value of the harvester efficiency is found from Eqs. (16)–(18) as [19]

$$\overline{\mathcal{C}_{\mathbb{P}}}(\tau) = \mathbb{E}\left[\frac{\mathrm{P}_{\mathrm{out}}(\tau)}{\mathrm{P}_{\mathrm{in}}(\tau)}\right] \approx \theta_{\mathbb{P}}(\tau)\frac{\mathbb{E}\left[\imath^2(\tau)\right]}{\sigma_\alpha(\tau)} \tag{19}$$

with the scalar, deterministic quantity $\theta_{\mathbb{P}}(\tau)$ [19]

$$\theta_{\mathbb{P}}(\tau) = \frac{2k_\alpha^3\Phi^2_{(\mathrm{e.m.c.})}}{(R_C)\rho b^2\ell\omega_\alpha\Pi^3(\tau)\bar{g}_{\alpha,T}} = \frac{k_\alpha^3\Psi^2 I_{0\alpha}}{2\rho b^4\ell\Pi^3(\tau)\bar{g}_{\alpha,T}} \tag{20}$$

The two expressions of Eq. (20), the right-hand side and the center side, are equivalent [19].

In Eq. (19) the dimensionless parameter $\theta_{\mathbb{P}}(\tau)$ depends on to geometry, structural dynamic properties of the harvester and Ψ. Equation (19) can be numerically determined by Monte Carlo methods, similarly to Secs. 5.3 and 6.1, i.e., by collecting a suitable sample of numerical solutions of Eq. (11) and subsequently evaluating the nonstationary mean square $\mathbb{E}[\imath^2(\tau)]$ and the nonstationary $\sigma_\alpha(\tau)$.

By comparing Eqs. (18)–(20) the expression of the mean, instantaneous output power is

$$\mathbb{E}[\mathrm{P}_{\mathrm{out}}(\tau)] = \omega_\alpha^3\Psi I_{0\alpha}\mathbb{E}[\imath^2(\tau)] \tag{21}$$

6.3 Quality (Q)-Factor. The Q-factor is often used to evaluate the performance of miniature harvesters, especially for micromechanical sensor design [62,63]. Since miniature, vibration-based harvesters are usually low-performing in comparison with large-scale, standard energy engineering apparatuses [e.g., Ref. 1], this quantity is preferably employed.

This quantity is also preferable to describe the output power in the case of resonant, linear harvesters with a fixed characteristic frequency that is constant. In this case, a constant vibration frequency yields a narrow-band response, which is associated with a high Q-factor and high peak power extraction [62].

The Q-factor is a dimensionless scalar, defined as [62,63] $Q(\tau) = \frac{1}{2[\zeta_\alpha + \zeta_{\mathrm{e.m.}}]}$, i.e., it is the inverse of the total damping ratio, combining the "parasitic" [63] or intrinsic [64], structural damping ratio ζ_α with the electric damping ratio $\zeta_{\mathrm{e.m.}}(\tau)$. More generally, $\zeta_{\mathrm{e.m.}}$ depends on the ability to convert and store the kinetic energy from the flow to electric energy. Nevertheless, the definition of Q-factor usually implies linear, frequency-domain analysis at resonance under harmonic excitation [62] that enables simple, closed-form estimation of this factor. In the case of steady-state, sustained periodic flapping at a constant angular amplitude, $\zeta_{\mathrm{e.m.}}$ is constant and can be found from the dimensional equation below:

$$\left\langle \mathrm{P}_{\mathrm{out}}(\tau)\right\rangle = \frac{1}{2\pi/\omega_\alpha}\int_0^{\frac{2\pi}{\omega_\alpha}}(2I_{0\alpha}\zeta_{\mathrm{e.m.}}\omega_\alpha)\left(\frac{\mathrm{d}\alpha}{\mathrm{d}t}\right)^2\mathrm{d}t = \left(2\sigma_\alpha^2\right)I_{0\alpha}\zeta_{\mathrm{e.m.}}\omega_\alpha^3 \tag{22}$$

where $\left\langle \mathrm{P}_{\mathrm{out}}(\tau)\right\rangle$ is the constant average output power, found by integration over one flapping period ($2\pi/\omega_\alpha$) and ($2\sigma_\alpha^2$) is the flapping amplitude squared.

Contrary to the standard definition used in the literature [62,63], $\zeta_{\mathrm{e.m.}}$ should be time-dependent since the Q-factor must assess the performance during nonstationary thunderstorms. Furthermore, the torsional harvester is nonlinear, stochastic and the excitation is a random noise. Therefore, the standard results [62,63] are not applicable. The Q-factor must be rewritten as

$$Q(\tau) = \frac{1}{2\left[\zeta_\alpha + \left\langle\zeta_{\mathrm{e.m.}}(\tau)\right\rangle\right]} \tag{23}$$

where the operator $\langle.\rangle$ designates temporal average, carried out over a suitable temporal duration, e.g., one flapping period, equal to 2π in dimensionless time units.

Equation (23) is a more suitable quantification of the Q-factor since it relies on the evaluation of electric damping through temporal averages, i.e., the energy due to fluid (aerodynamic) losses and absorbed by the power system [64]. Equation (23) can also account for other uncertainty sources (i.e., loading) and is compatible with Eq. (21) for this harvester. Equation (23) is still approximate since it requires ergodicity to compute the temporal average of the aerodynamic damping over a suitable temporal duration, i.e., one full vibration cycle by similarity with Eq. (22). Therefore, the time-averaged electric damping in Eq. (23) is evaluated for nonstationary, random flapping as

$$\left\langle\zeta_{\mathrm{e.m.}}(\tau)\right\rangle = \frac{\mathbb{E}[\mathrm{P}_{\mathrm{out}}(\tau)]}{2\sigma_\alpha^2(\tau)I_{0\alpha}\omega_\alpha^3} = \frac{\Psi\mathbb{E}\left[\imath^2(\tau)\right]}{2\sigma_\alpha^2(\tau)} \tag{24}$$

where Eq. (21) is utilized along with the instantaneous expected values, which evaluate the output power and the standard deviation of the flapping angle at time τ.

It must be noted that nonlinear dissipation in structural dynamics may alternatively be estimated through a "more classical" approach [65], although the latter approach is not pursued herein.

Furthermore, alternative definitions of Q-factor are possible, for example, considering the maximum electric damping ratio, attained during nonstationary excitation. Nevertheless, Eqs. (23) and (24) are still preferable for comparison purposes with other harvesters, based on micromechanical systems [62,63].

7 Moment Lyapunov Exponent Results

7.1 Description of the Apparatuses. Simulations examine an apparatus with rotation pivot axis at the apex of the blade-airfoil ($a = -1$) and AR = 4 ($\ell = 4b$). Three "Types" are selected from Ref. [11], with the main properties described in Table 1, in which quantities such as angular frequency and damping ratio must be

interpreted as the properties of the linearized dynamic equation of the harvester.

The nonlinear stiffness parameter in the Duffing model (Eq. (9)) is constant and set to $\kappa = 100$, irrespective of the type. Similarly, a variable nonlinear damping parameter $\gamma > 0$ is used in the Hybrid Duffing–van-der-Pol model (Eq. (10)).

Coupling with the power circuit is achieved by setting $\Psi = 0.01$ and $\lambda_{RL} = 0.75$ [11].

Finally, initial conditions are imposed by considering an initial flapping angular motion at $\tau = 0$, needed to trigger the instability [11]. The initial amplitude of α is set to random with zero mean and standard deviation equal to 2 deg, coincident with small, realistically plausible angular deviations from the static equilibrium.

Numerical solution of Eq. (11) is repeated 200 times by Monte Carlo sampling and step-by-step integration to find the relevant moments in weak form [23].

7.2 Duffing Model

7.2.1 Frozen Thunderstorm Downburst. This scenario corresponds to the reference condition for a structurally linear harvester (Eq. (9) with $H_{NL} = 0$), found under the hypothesis of "frozen thunderstorm state," i.e., a stationary, turbulent flow field with time-independent, constant mean speed $U = U_{max}$ [$\Pi(\tau) = 1$ and $\varphi_{mf}(\tau) = 1$] and low turbulence. As discussed in a recent study [19] and contrary to [25], it is useful to examine this case to determine incipient flutter condition, signaled by a definitely positive $\Lambda_\Upsilon(2) > 0$ since unstable, diverging torsional flutter is only possible. By contrast, the study of a case including either Eq. (9) or Eq. (10) with $H_{NL} \neq 0$ may still lead to a stable, postcritical flapping with a limit cycle that can still exhibit a negative or a "nearly zero" MLE [19].

Following recent numerical results [19], initial harvester simulations are executed in the range $0 < U_{max} \leq 20$ m/s since this range exhibits flutter. Furthermore, the harvester efficacy at moderate wind speeds is the primary goal of the design. Although less controllable buffeting vibrations are possible at the same wind speeds because of flow turbulence, flapping may be blocked to avoid damaging the apparatus.

Figure 3 illustrates an example of the reference scenario with linear, structural harvester and Eq. (9) with $H_{NL} \approx 0$, found by setting $\kappa = 10^{-7}$ and numerically solving Eq. (15). Results are shown for frozen thunderstorm state with constant U [$\Pi(\tau) = 1$ and $\varphi_{mf}(\tau) = 1$] and low turbulence of standard deviation $\sigma_{\hat{u}} = 2\%$. Load perturbation is also accounted for.

The standard deviation of the random load in Fig. 3 is $\sigma_{d2} = 0.07$. Type 2 apparatus is unstable at $U = 14.4$ m/s, noting that $\Lambda_\Upsilon(2) > 0$ diverges for $\tau > 100$ in Fig. 3(*b*). Other apparatuses do not exhibit any unstable behavior in the examined range of mean flow speeds.

7.2.2 Active Thunderstorm Downburst. Figure 4 depicts the intensification and modulation functions, applied to the "active thunderstorm state." This figure shows the two functions for a short thunderstorm of total duration $T \approx 600$ s [35], i.e., $\tau_{max} = 190$, typical of short-lived thunderstorms over complex terrain in urban settings [36]. This example demonstrates the nonideal flow conditions that are likely to further reduce the propensity of the harvester to flapping [19].

In Fig. 4 the mean outflow intensity varies with $\Pi(\tau)$ as $U_{max}\Pi(\tau)$ while the zero-mean random turbulence $\hat{u}$ is modulated with $\varphi_{mf}(\tau)$. The special normalization used in Eq. (2) leads to a φ_{mf} function

Table 1 Harvester and thunderstorm properties

Type	b (m)	$\frac{I_{0\alpha}}{\ell}\left(\frac{\text{kgm}^2}{\text{m}}\right)$	$\frac{\omega_\alpha}{2\pi}$ (Hz)	ζ_α (%)	AR	τ_{max}
0	0.25	20	0.25	0.25	4	190
1	0.25	40	0.25	0.30	4	190
2	0.50	300	0.10	0.30	4	190

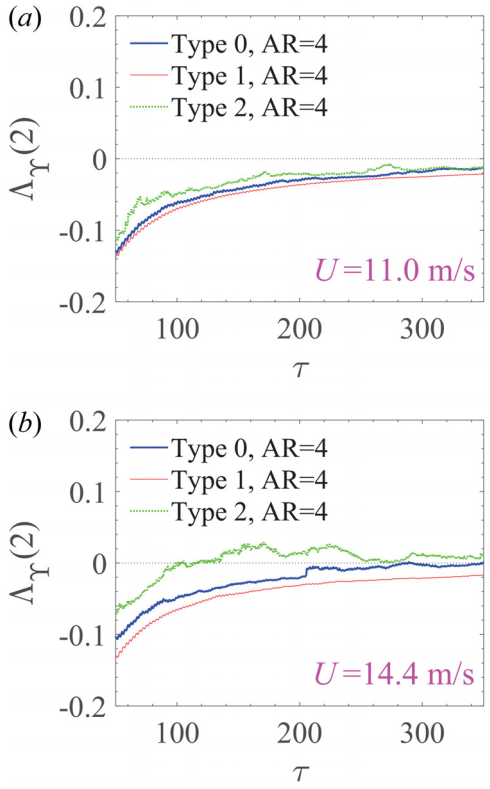

Fig. 3 Frozen thunderstorm with turbulence of intensity $\sigma_{\hat{u}}$=2% and aeroelastic load perturbation σ_{d2}=0.07: $\Lambda_\Upsilon(2)$ versus time τ for a structurally-linear harvester at (*a*) U = 11.0 m/s and (*b*) U = 14.4 m/s. Reproduced with permission from Ref. [19]. Copyright © 2024 by Elsevier.

with sharp turbulence intensity variations around τ_{max} (dashed-dotted line in Fig. 4), while the mean outflow field is accompanied by a smoother transition (continuous line in Fig. 4). Furthermore, the effect of turbulence on instability onset in Fig. 4 vanishes at about $\tau \approx 300$, with $\varphi_{mf} \approx 0$. Therefore, any unstable flapping observed beyond $\tau \approx 300$ is triggered by a load in a predominantly smooth flow.

Finally, φ_{mf} does not depend on $\sigma_{\hat{u}}$ in Fig. 4. However, its sharpness is influenced by ω_α in accordance with Eq. (2), i.e., it reproduces the flow conditions primarily for a Type-2 apparatus with $\omega_\alpha = 0.628$ rad/s. Nevertheless, the latter dependency is only apparent, i.e., a consequence of the normalization used in Eq. (8).

It is also noted in Fig. 4 that the effective duration of the function $\Pi(\tau)$ is longer than the turbulent part (or the gust front), i.e., $\varphi_{mf}(\tau)$.

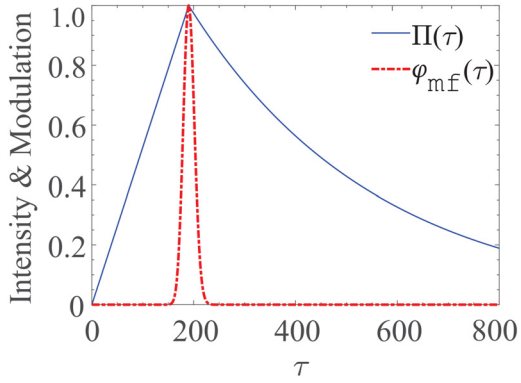

Fig. 4 Active thunderstorm's temporal functions of the mean outflow $\Pi(\tau)$, and turbulence $\varphi_{mf}(\tau)$ (τ_{max}=190, ω_α=0.628 rad/s)

Since the translation velocity of the thunderstorm is neglected in the formulation (Eq. (3)), the mean flow velocity is modulated on $\Pi(\tau)$ that represents evolution of the storm over its duration T. This difference may be eliminated by parametrizing Eq. (1). Further investigation is needed although it is beyond the scope of the study.

Similarly, if the definition of mean-square stability is considered [23,50], the asymptotic condition ($\tau \to +\infty$) in Eq. (15) is less meaningful as $\Pi(\tau)$ tends to zero with consequent vanishing of the load. Rather, incipient instability should possibly be referred to the fully-developed thunderstorm gusty wind. Consequently, the empirical evaluation by Eq. (15) at about $\tau_l \approx 300$ is adequate; in other words, $\Lambda_{\Upsilon}(2) > 0$ can still be used to detect a transitory unstable regime if a linear harvester model is used. This observation is discussed below in Fig. 5.

Caracoglia [19] recently demonstrated that the temporal intensification of the thunderstorm, i.e., the time-varying, slowly-varying mean wind speed $U(\tau)$ with $\Pi(\tau) \neq 1$ is detrimental to this apparatus, mainly influences its stability and extends the flapping onset beyond 20 m/s. Furthermore, high turbulence with $\sigma_{\hat{u}} = 10\%$ is desirable to trigger flutter. As an example, Fig. 5 analyzes the mean-square stability of the harvester for an active turbulence state with $\sigma_{\hat{u}} = 10\%$, i.e., the turbulence intensity is five times larger than the one used in Fig. 3.

Figure 5 compares the MLE empirically found with linear apparatus (a), and nonlinear Duffing model (b).

First, higher turbulence is necessary since no instability has been found numerically in any foreseeable range of $U_{\max}$ if an active thunderstorm is considered. Additional evidence may be found in a recent study [19]. In Fig. 5 the combination of low turbulence and decreasing mean aeroelastic load proportional to $\Pi(\tau)^2$ at about $\tau_{\max} = 190$ contribute to a harvesting performance loss.

Second, Type-2 apparatus becomes incipiently unstable (i.e., flutter onset) at $U_{\max} = 27.0$ m/s, depicted in Fig. 5(*a*), since $\Lambda_{\Upsilon}(2) > 0$ diverges at about $\tau = 200$, with the numerically evaluated $\Lambda_{\Upsilon}(2)$ fluctuating about the zero axis. A "marginally" unstable trend $\Lambda_{\Upsilon}(2) > 0$ is possibly noticeable for Type-0 apparatus in Fig. 5(*a*) at about the same τ.

Third, the nonlinear Duffing model with $H_{NL} \neq 0$ in Fig. 5(*b*) exhibits a permanently stable MLE trend for all cases. This observation is plausible with the occurrence of limit-cycle sustained flapping [19], at least for Type-2 apparatus. Employing a linear harvester model is, therefore, more suitable to detect (and compare) incipient instability condition, while energy conversion and Sec. 6 must be considered to evaluate the performance of the harvester beyond any unstable limit.

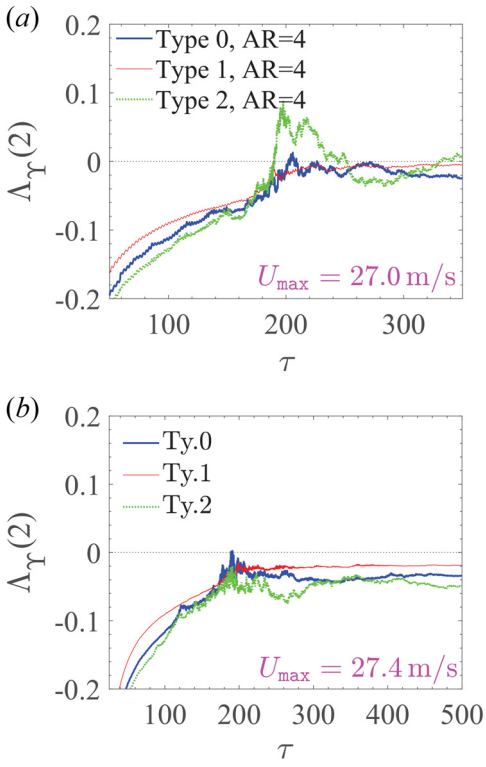

Fig. 5 Active thunderstorm with high turbulence of intensity $\sigma_{\hat{u}}$=10% and aeroelastic load perturbation σ_{d2}=0.07: $\Lambda_{\Upsilon}(2)$ versus time τ at $U_{\max} \approx 27$ m/s and a harvester model: (*a*) linear (κ=10^{-7}) and (*b*) nonlinear Duffing with $\kappa = 100$ in Eq. (9) ["Ty." = Type].

7.3 Duffing – Van-der-Pol Model

7.3.1 Foreword. The nonlinear damping parameter γ is varied to evaluate the sensitivity of the apparatus to this new hybrid model feature (Eq. (10)). Several configurations are investigated with $\gamma = \{0.2, 0.5, 1, 30, 300\}$, some of which are unrealistic. At the same time $\kappa = 100$ is utilized throughout Sec. 7.3 to allow comparisons with Sec. 7.2 and, more specifically, Fig. 5.

An initial pilot test is also carried out by numerically studying a simplified case of an absolutely stable nonlinear Duffing–van-der-Pol model oscillator, in which the aeroelastic load is set to zero and a random, stationary buffeting torque is introduced as external buffeting only. The results of this test are not shown for the sake of brevity. The general remark is that nonlinear oscillators with $\gamma = \{0.2, 0.5, 1\}$ and $\kappa = 100$ are numerically solvable by step-by-step integration [51]. On the contrary, not only are larger γ values more questionable from the physical point of view, $\gamma > 1$ may also yield a "stiff" nonlinear differential equation that can successfully be solved by a more specialized numerical method. Consequently, the Euler-Monte Carlo solver [51], used in Eq. (11), may lead to erroneous, numerically induced unstable solution that is noted in Ref. [19] but not in Ref. [25].

7.3.2 Frozen Thunderstorm Downburst. From the remarks noted in Sec. 7.2, simulations are limited to high turbulence, active thunderstorm state ($\sigma_{\hat{u}} = 10\%$).

It is observed that, in general, the addition of the new damping feature in the model does not induce relevant changes to the stochastic instability and operational conditions of the apparatus, compared to the Duffing model in Sec. 7.2, with somehow little influence of the damping parameter $\gamma = 1$ on the graphs of $\Lambda_{\Upsilon}(2)$.

As an example, Fig. 6 presents the results for the new hybrid model subject to a high turbulence, stationary, or frozen thunderstorm state with constant mean flow, $U_{\max} = U$. The figure essentially replicates the same trends exhibited in Fig. 5(*a*) with nonlinear Duffing model: stable apparatus at $U = 11.0$ m/s and unstable-operational apparatus at about $U = 16.4$ m/s in Fig. 6(*b*). Both Type-2 and Type-0 apparatuses appears to be operational. In fact, in Fig. 6(*b*) the MLE $\Lambda_{\Upsilon}(2)$ crosses the zero axis and becomes positive at $\tau = 140$ for Type-0 apparatus (thick solid line), while $\Lambda_{\Upsilon}(2) > 0$ of Type-2 apparatus is already strongly positive at $\tau = 50$ (dotted line, visible on the left side of the graph).

Nevertheless, a sudden "jump" in the thick solid line, describing the behavior of Type-0 apparatus in Fig. 6(*b*), is noticeable at about $\tau = 145$ with a clear, vertical asymptote [$\Lambda_{\Upsilon}(2) \to +\infty$]. This "explosion" of $\Lambda_{\Upsilon}(2)$ is plausibly unrealistic, by careful inspection of the definition in Eq. (15), possibly contaminated by numerical integration issues. A similar issue was observed in a recent study [19], in which some additional discussion is provided that attributes the problem to the Euler's numerical solver [51].

7.3.3 Active Thunderstorm Downburst. The graphs $\Lambda_{\Upsilon}(2)$ versus time are presented in Fig. 7 for an active, nonstationary high turbulence thunderstorm. To extend the evaluation of the damping feature, $\gamma = 0.5$ is also considered; the proposed decrement by a factor of two compared to Fig. 6 is acceptable from a physical perspective. For instance, larger γ values have been hypothesized; a large value $\gamma = 300$ was preliminarily investigated in Ref. [25] to scrutinize a wider range of options. Nevertheless, the

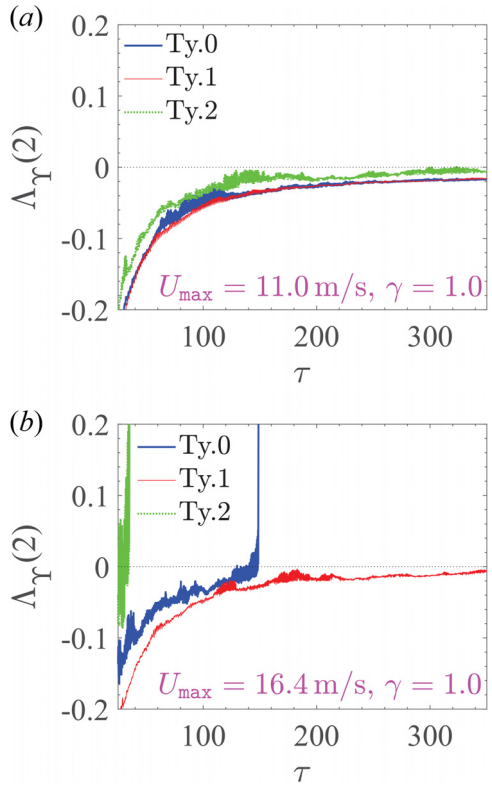

Fig. 6 Nonlinear hybrid Duffing – van-der-Pol model with γ=1.0 subject to frozen thunderstorm with turbulence of intensity $\sigma_{\dot{u}}$=10% and aeroelastic load perturbation with σ_{d2}=0.07. $\Lambda_\Upsilon(2)$ versus time at (*a*) U = 11.0 m/s and (*b*) U = 16.4 m/s ["Ty." = Type].

hybrid harvester case with $\gamma > 1$ was not considered in this study as it is possibly unrealistically large, less meaningful to design.

The graphs $\Lambda_\Upsilon(2)$ versus time, presented in Fig. 7, refer to slowly-varying mean wind speed with $U \approx 27$ m/s. Contrary to Sec. 7.3.2, the $\Lambda_\Upsilon(2)$ numerical analysis is extended to $\tau_l = 500$. Figure 7 tends to confirm the remarks in Sec. 7.2.2. Nevertheless, flutter instability is temporarily engaged at about $\tau_l \approx \tau_{max} = 190$ for Type-2 apparatus in Fig. 7(*a*) with a lower $\gamma = 0.5$ with $\Lambda_\Upsilon(2) > 0$, whereas the transient unstable trend disappears in Fig. 7(*b*) with a larger $\gamma = 1.0$. Other apparatus' types are not affected. The MLE graphs are, however, similar to the behavior observed in Fig. 5(*b*), corroborating the observation that output power analysis is necessary to study postcritical flutter performance.

8 Stochastic Output Power Results

Output power analysis is based on the numerical evaluation of output power coefficient in Eq. (20), mean output power in Eq. (22) and Q-factor by Eqs. (23) and (24). Primary consideration is given to the nonideal, nonstationary thunderstorm flow conditions and the hybrid Duffing–van-der-Pol model. Preliminary investigation on stochastic output power during post-critical stages for the Duffing model and apparatus are reported in a recent study [19] and are briefly summarized only in this paper.

8.1 Duffing Model (Nonstationary Flows Only). In this scenario, Type-2 apparatuses is engaged at about $U_{max} = 27.4$ m/s (Fig. 5) during post-critical flutter; Type-0 is also possibly operational while Type-1 is not triggered. Figure 8 illustrates the power results and examines $\overline{\mathcal{C}_{\mathbb{P}}}(\tau)$, $\mathbb{E}[P_{out}(\tau)]$ and Q-factor. In Figs. 8(*a*) and 8(*b*), energy conversion in only visible at time $190 < \tau < 300$, compatible with the maximum intensification of the nonstationary flow (Fig. 4). Although Type-0 apparatus has a noticeable efficiency compared to Type-2, the energy conversion is still quite low in terms of $\mathbb{E}[P_{out}(\tau)]$. Furthermore, the efficiency measured by $\overline{\mathcal{C}_{\mathbb{P}}}(\tau)$ is of the order of 10^{-4} and it is meaningless in comparison with the output power coefficient of large-scale wind energy systems [66]. Energy conversion appear to be active although the average output power is low (Fig. 8(*a*)).

In Fig. 8(*c*) the graphs compare the time-dependent Q-factor to the corresponding inactive scenario, in which the Q-factor tends to its upper limit $Q(\tau) = Q = 1/(2\zeta_x)$ since Eq. (25) is set to zero. The latter case is portrayed in the figure by a dotted horizontal line, e.g., $Q = 166.\bar{6}$ for Type-1 and Type-2 apparatuses (Table 1). Typically in a miniature device, a good achievement can be associated with a condition, in which the Q-factor is as large as possible [63] and avoids prevailing parasitic effects. Since the proposed apparatus is not a traditional miniature harvester, any remark should be carefully considered. Therefore, in the case of Fig. 8(*c*), the "quality" can be achieved if $Q(\tau)$ is approximately constant over time. Unfortunately, this is not noticeable, at least from the numerical results; undesirable fluctuations are visible during both the primarily active stage ($190 < \tau < 300$) and the subsequent decay of the thunderstorm flow effects. In particular, the quality rapidly "switches" between 0 and the upper limit, clear indicator of a nonideal, deficient performance.

8.2 Hybrid Duffing–Van der Pol Model. Figure 9 presents the output power analysis results of Duffing–van-der-Pol model apparatus with $\gamma = 0.5$, $\kappa = 100$ under active thunderstorm outflows. The results in Fig. 9 may be compared against those in Fig. 8. In each figure panel the value of γ parameter is indicated as a label to differentiate the graphs from the Duffing model case ($\gamma = 0$, Fig. 8). While the vertical axis scales of $\overline{\mathcal{C}_{\mathbb{P}}}(\tau)$ and Q-factor are the same, the scale of $\mathbb{E}[P_{out}(\tau)]$ in Fig. 9(*a*) is larger to discern the differences. Clearly, the nonlinear damping effect, introduced with H_{NL} in Eq. (10), is beneficial. A moderate $\gamma = 0.5$ nonlinearity produces a remarkable relative increment in the average output power at time $200 < \tau < 300$, especially for Type-2 apparatus. Type-2's

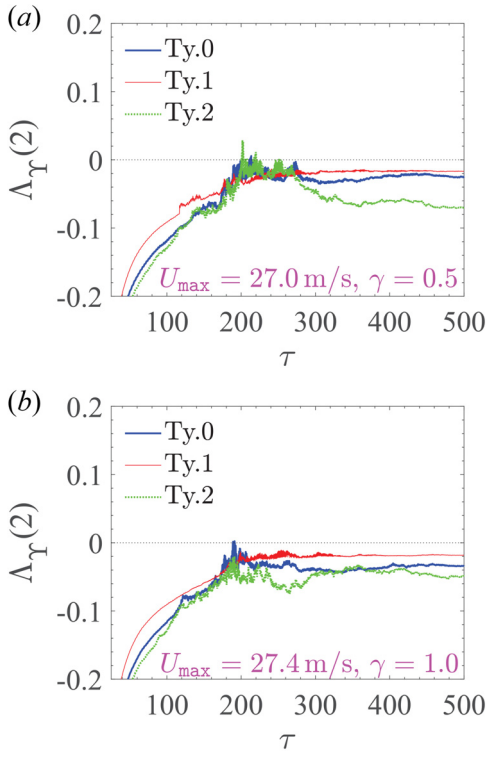

Fig. 7 Nonlinear hybrid Duffing – van-der-Pol Model with variable γ (*a*) γ=0.5 and (*b*) γ=1.0, subject to nonstationary active thunderstorm with turbulence of intensity $\sigma_{\dot{u}}$=10% and aeroelastic load perturbation with σ_{d2}=0.07. $\Lambda_\Upsilon(2)$ versus time at $U \approx$ 27 m/s ["Ty." = Type].

achievable power conversion seems more efficient, although the absolute value of $\mathbb{E}[P_{out}(\tau)]$ is still low and despite the dimensions of the blade-airfoil (Table 1).

Nevertheless, the favorable behavior of Type-2 harvester is much less evident if one compares $\overline{\mathcal{C}_{\mathbb{P}}}(\tau)$ in Fig. 9(*b*). The reason is believed to be related to the concurrent small values of the term $\theta_{\mathcal{P}}(\tau)$, accompanied by large $\sigma_{\alpha}(\tau)$ in Eq. (19). This remark confirms previous evidence [19] and suggests that the definition of $\overline{\mathcal{C}_{\mathbb{P}}}(\tau)$ may be inappropriate for the purposes of comparing performance. Furthermore, the Q-factor is a similarly unsuitable indicator, although some difference is noticeable by considering the expectations, i.e., the temporal average of $Q(\tau)$ in Fig. 9, which suggests a slight preference of Type-0 versus Type-2 apparatus because of a moderately larger average.

Finally, $\mathbb{E}[P_{out}(\tau)]$ is analyzed in the case of frozen downburst storm, i.e., stationary turbulent wind field with constant mean speed U. The special case at $U = 14.0$ m/s is illustrated. These results, presented in Fig. 10 for a Duffing–van-der-Pol model harvester with $\gamma = 1.0$, can possibly be examined against Fig. 9(*a*) of the nonstationary case at $U_{max} = 27.0$ m/s. The graphs are limited to the time interval $25 < \tau < 250$. The average output power,

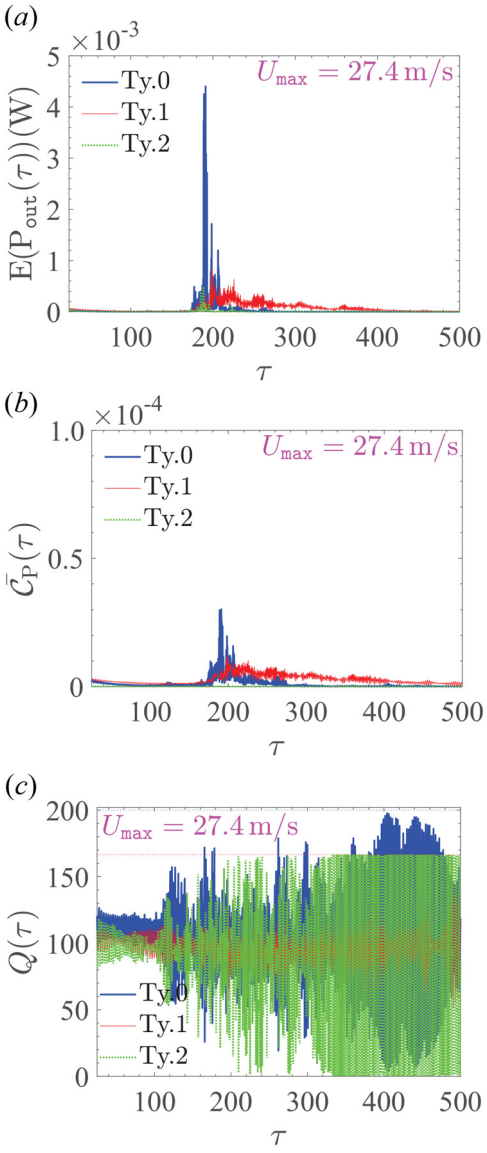

Fig. 8 Output power analysis of Duffing model harvester with $\kappa = 100$, subject to nonstationary active thunderstorm of intensity $\sigma_{\dot{u}}$=10% and U_{max}=27.4 m/s, and aeroelastic load perturbation with σ_{d2}=0.07: (*a*) $\mathbb{E}[P_{out}(\tau)]$ average output power, (*b*) $\overline{\mathcal{C}_{\mathbb{P}}}(\tau)$ mean output power coefficient, and (*c*) Q-factor ["Ty." = Type]

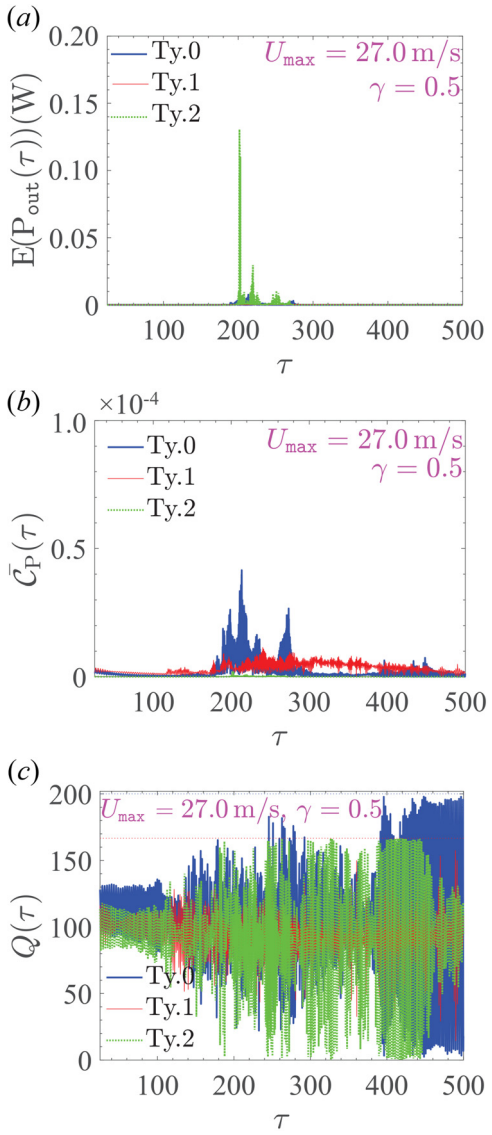

Fig. 9 Output power analysis of Duffing – van-der-Pol model harvester with γ=0.5, $\kappa = 100$, subject to nonstationary active thunderstorm of intensity $\sigma_{\dot{u}}$=10% and U_{max}=27.0 m/s, and aeroelastic load perturbation with σ_{d2}=0.07: (*a*) $\mathbb{E}[P_{out}(\tau)]$ average output power, (*b*) $\overline{\mathcal{C}_{\mathbb{P}}}(\tau)$ mean output power coefficient, and (*c*) Q-factor ["Ty." = Type]

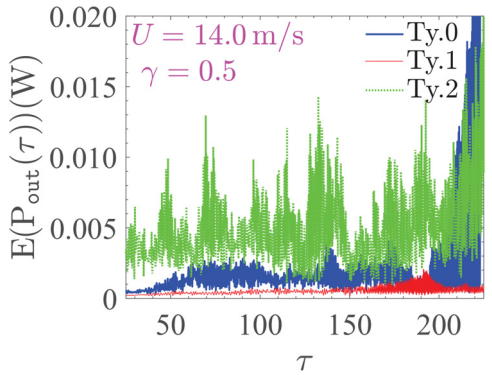

Fig. 10 Average output power $\{\mathbb{E}[P_{out}(\tau)]\}$. of a Duffing – van-der-Pol model harvester with γ=0.5, $\kappa = 100$, subject to a frozen thunderstorm with turbulence of intensity $\sigma_{\dot{u}}$=10% and a constant outflow speed $U = 14.0$ m/s ["Ty." = Type].

achievable during a low-speed stationary boundary layer wind with Type-2 apparatus (thick dotted line), exhibits a much larger value compared to Fig. 9(*a*). Moreover, non-negligible output power is also noted for Type-0 device. Less promising conversion powers are, however, attainable during nonideal outflow conditions. Additional investigations, beyond the scope of this study, are advisable to simultaneously optimize the parameters γ and κ in Eq. (10) of the hybrid model.

9 Conclusions

Numerical investigations confirm the detrimental effect of nonideal flows with, on average, an adverse increment of operational flutter speed above +30%. Nevertheless, the proposed implementation of a hybrid restoring torque mechanism coupled with nonlinear damping effect ($\gamma = 0.5$) is promising, since the achievable power conversion may possibly be one order of magnitude larger; this beneficial effect is observed at very large values of critical $U_{\max}$, Besides the parameter γ, flutter propensity is mainly controlled by α^2 in the van-der-Pol equation. Since amplitudes of the flapping angular motion are moderate at sustained and benign flutter, activation of this effect is further exacerbated by the nonstationary flow conditions and imperfect fluid–structure interaction. Consequently, a successful exploitation of the proposed apparatus is still dubious during nonstationary wind events.

Additional investigation is still needed to better characterize the role of the hybrid Duffing–van-der-Pol model in the context of practical design. Verification and validation by wind tunnel tests are also advisable to confirm the observations. Furthermore, exploitation of nonlinear aeroelastic loads ([67]) should be considered to more realistically reproduce the loads at moderate flapping amplitudes. Finally, even though flutter speed can be found in closed form in the absence of turbulence and other random perturbations, the same approach could be pursued to examine mean-square stability through approximation of the nonlinear equation solutions, e.g., by stochastic approximation.

Acknowledgment

Any opinions, findings, and conclusions or recommendations are those of the author and do not necessarily reflect the views of the NSF.

Funding Data

- National Science Foundation (NSF) of the United States of America (Award No. CMMI-2020063; Funder ID: 10.13039/100000084).

Conflict of Interest

The author declares that he has no known competing financial interests or personal relationships that could have appeared to influence the work reported in this paper.

Data Availability Statement

Data and models that support the findings of this study are available from the corresponding author upon reasonable request.

Nomenclature

a = dimensionless position of the pivot "O"
AR = aspect ratio of the blade-airfoil
b = half-chord width of the blade-airfoil
$B_{\hat{u}}(\tau)$ = scalar Wiener noise for turbulence perturbation
$B_{\Delta 2}(\tau)$ = scalar Wiener noise for load perturbation
c_i = amplitude parameters of the Φ function ($i = 1, 2$)
d_i = exponent parameters of the Φ function ($i = 1, 2$)
$d_{2,\mathrm{m}}$ = mean value of random exponent parameter d_2
$g_{\alpha,T}(\tau)$ = random peak factor of α
$\bar{g}_{\alpha,T}(\tau)$ = expected value of the random peak factor of α
$\mathrm{H_{NL}}(\alpha, \mathrm{d}\alpha/\mathrm{d}\tau)$ = nonlinear restoring mechanism forcing function
$I(\tau)$ = output current of the power system (A)
I_{0z} = polar mass moment of inertia of the flapping foil (kgm^2)
k_α = reduced frequency of the 1DOF flapping foil
ℓ = span-wise longitudinal length of the blade-airfoil
L_C = impedance of output power circuit (Henries)
M_{0z} = aeroelastic torque (Nm)
$M_{(\mathrm{e.m.})}$ = electromotive torque (Nm)
$\mathrm{P_{in}}(\tau)$ = input power of the wind flow
$\mathrm{P_{out}}(\tau)$ = output power of the harvester
$Q(\tau)$ = quality factor
$\mathbf{Q}_{\mathrm{L},\Delta 2}$ = diffusion matrix of the load perturbation
$\mathbf{q}_{\mathrm{em,NL}}(\mathbf{W}_{\mathrm{em}})$ = nonlinear drift vector-function
R_C = resistance of output power circuit (Ohms)
$S_{\hat{u}}$ = spectrum of dimensionless, stationary turbulence
$S_{\hat{u},\mathrm{EPSD}}$ = evolutionary spectrum of non-stationary turbulence
t = rime (s)
$t_{\max}$ = time (s), downburst's maximum intensification
$\mathbf{t}_{\mathrm{NL},\hat{u}}$ = nonlinear turbulence diffusion function
T = total effective duration of the thunderstorm (s)
$u(\tau)$ = along-wind non-stationary turbulence (m/s)
$U(\tau)$ = "mean" outflow wind speed (m/s)
$U_{\max}$ = maximum slowly-varying wind speed (m/s)
$\hat{u}(\tau)$ = normalized along-wind non-stationary turbulence
$\mathbf{W}_{\mathrm{em}}(\tau)$ = random state vector
$\boldsymbol{\Upsilon}$ = sub-vector of random vector $\mathbf{W}_{\mathrm{em}}$
z = vertical axis coordinate
$z_{\max}$ = height, maximum downburst intensification
α = flapping angle of the blade-airfoil, about pivot "O"
α_{pk} = Peak flapping angle process from parent α
γ = nonlinear damping, Duffing-van der Pol model
δ_2 = random perturbation to mean parameter $d_{2,\mathrm{m}}$
ϵ = normalized inertia parameter
ζ_α = structural damping of the flapping foil
$\eta_{3\mathrm{D}}$ = parameter for three-dimensional load effects
$\theta_{\mathbb{P}}(\tau)$ = scalar, deterministic parameter of output power
$\imath$ = dimensionless induced current of the power circuit
κ = dimensionless stiffness, nonlinear restoring torque
$\Lambda_{\boldsymbol{\Upsilon}}(2)$ = second moment Lyapunov exponent
λ_{RL} = generalized impedance of the power circuit
$\mu_{ae,i}(\tau)$ = aeroelastic state ($i = 1, 2$)
$\nu^+_{0\alpha}$ = rate of α zero up-crossings
$\nu_{ae,i}(\tau)$ = aeroelastic state ($i = 1, 2$)
$\Pi(\tau)$ = temporal intensification function
ρ = air density
σ_α = standard deviation of α
σ_{d2} = standard deviation of $\delta_2(\tau)$
$\sigma_{\hat{u}}$ = standard deviation of $\hat{u}$
τ = dimensionless time, $\tau = t\omega_\alpha$
τ_l = discrete time instant, used to estimate MLE
$\tau_{\max}$ = dimensionless time, maximum intensification
Φ = unsteady aeroelastic forcing function
Φ_0 = unsteady aeroelastic forcing function at $\tau = 0$
$\Phi_{(\mathrm{e.m.c.})}$ = dimensional electro-mechanical coupling
$\varphi_{\mathrm{mf}}(\tau)$ = modulation function for downburst's $S_{\hat{u},\mathrm{EPSD}}$
Ψ = dimensionless electro-mechanical coupling coeff
ω = angular vibration frequency (rad/s); and
ω_α = pulsation of the one-DOF flapping foil (rad/s)

Abbreviations and Operators

DOF = degree-of-freedom
$\mathbb{E}[.]$ = expectation operator

MLE = moment Lyapunov exponent
$\langle \cdot \rangle$ = temporal average
$[.]^T$ = transpose operator

References

[1] Priya, S., and Inman, D. J., 2009, *Energy Harvesting Technologies*, Springer Science, New York.
[2] Matsumoto, M., Mizuno, K., Okubo, K., and Ito, Y., 2006, "Fundamental Study on the Efficiency of Power Generation System by Use of the Flutter Instability," ASME Paper No. PVP2006-ICPVT11-93773.
[3] Pigolotti, L., Mannini, C., Bartoli, G., and Thiele, K., 2017, "Critical and Post-Critical Behaviour of Two-Degree-of-Freedom Flutter-Based Generators," J. Sound Vib., **404**, pp. 116–140.
[4] Singh, K., Michelin, S., and de Langre, E., 2012, "Energy Harvesting From Axial Fluid-Elastic Instabilities of a Cylinder," J. Fluids Struct., **30**, pp. 159–172.
[5] Eugeni, M., Elahi, H., Fune, F., Lampani, L., Mastroddi, F., Romano, G. P., and Gaudenzi, P., 2020, "Numerical and Experimental Investigation of Piezoelectric Energy Harvester Based on Flag-Flutter," Aerosp. Sci. Technol., **97**, p. 105634.
[6] Gkoumas, K., Petrini, F., and Bontempi, F., 2017, "Piezoelectric Vibration Energy Harvesting From Airflow in HVAC (Heating Ventilation and Air Conditioning) Systems," Proc. Eng., **199**, pp. 3444–3449.
[7] Petrini, F., and Gkoumas, K., 2018, "Piezoelectric Energy Harvesting From Vortex Shedding and Galloping Induced Vibrations Inside HVAC Ducts," Energy Build., **158**, pp. 371–383.
[8] Meshki, M. M., Nobari, A. S., and Sadr, M. H., 2022, "A Study on Nonlinear, Parametric Aeroelastic Energy Harvesters Under Oscillatory Airflow," J. Vib. Control, **28**(1–2), pp. 192–202.
[9] Bernitsas, M. M., Raghavan, K., Ben-Simon, Y., and Garcia, E. M. H., 2008, "VIVACE Vortex Induced Vibration Aquatic Clean Energy: A New Concept in Generation of Clean and Renewable Energy From Fluid Flow," ASME J. Offshore Mech. Arct. Eng., **130**(4), p. 041101.
[10] Le, H., Kwon, S.-D., and Law, K., 2023, "Hybrid Energy Harvesting From Wind and Bridge Vibrations," Proceedings of 16th International Conference on Wind Engineering (ICWE16), Florence, Italy, Aug. 27–31.
[11] Caracoglia, L., 2018, "Modeling the Coupled Electro-Mechanical Response of a Torsional-Flutter-Based Wind Harvester With a Focus on Energy Efficiency Examination," J. Wind Eng. Ind. Aerodyn., **174**, pp. 437–450.
[12] Ahmadi, G., 1979, "An Oscillatory Wind Energy Convertor," Wind Eng., **3**, pp. 207–215.
[13] Roohi, R., Hosseini, R., and Ahmadi, G., 2023, "Parametric Study of an H-Section Oscillatory Wind Energy Converter," J. Ocean Eng., **270**, p. 113652.
[14] Kwon, S.-D., Park, J., and Law, K., 2013, "Electromagnetic Energy Harvester With Repulsively Stacked Multilayer Magnets for Low Frequency Vibrations," Smart Mater. Struct., **22**(5), p. 055007.
[15] Solari, G., De Gaetano, P., and Repetto, M. P., 2015, "Thunderstorm Response Spectrum: Fundamentals and Case Study," J. Wind Eng. Ind. Aerodyn., **143**, pp. 62–77.
[16] Solari, G., 2016, "Thunderstorm Response Spectrum Technique: Theory and Applications," Eng. Struct., **108**, pp. 28–46.
[17] Solari, G., and De Gaetano, P., 2018, "Dynamic Response of Structures to Thunderstorm Outflows: Response Spectrum Technique versus Time-Domain Analysis," Eng. Struct., **176**, pp. 188–207.
[18] Nayfeh, A. H., and Mook, D. T., 1995, *Nonlinear Oscillations*, Wiley-VCH Verlag GmbH & Co. KGaA, Weinheim, Germany.
[19] Caracoglia, L., 2024, "Stochastic Performance of a Torsional-Flutter Harvester in Non-Stationary, Turbulent Thunderstorm Outflows," J. Fluids Struct., **124**, p. 104050.
[20] Pandey, M., Rand, R., and Zehnder, A., 2007, "Perturbation Analysis of Entrainment in a Micromechanical Limit Cycle Oscillator," Commun. Nonlinear Sci. Numer. Simul., **12**(7), pp. 1291–1301.
[21] Belhaq, M., Ghouli, Z., and Hamdi, M., 2018, "Energy Harvesting in a Mathieu-Van Der Pol-Duffing MEMS Device Using Time Delay," Nonlinear Dyn., **94**(4), pp. 2537–2546.
[22] Liu, D., Xu, S., and Ma, J., 2023, "Bayesian System Identification and Chaotic Prediction From Data for Stochastic Mathieu-Van Der Pol-Duffing Energy Harvester," Theor. Appl. Mech. Lett., **13**(2), p. 100412.
[23] Grigoriu, M., 2002, *Stochastic Calculus. Applications in Science and Engineering*, Birkhäuser, Boston, MA.
[24] Xie, W.-C., 2005, "Monte Carlo Simulation of Moment Lyapunov Exponents," ASME J. Appl. Mech., **72**(2), pp. 269–275.
[25] Caracoglia, L., 2023, "Stochastic Stability of a Torsional-Flutter Energy Harvester in Thunderstorm-Like Winds: Duffing vs. Hybrid Duffing – Van Der Pol Restoring Force Mechanisms," ASME Paper No. IMECE2023-116381.
[26] Kwon, D. K., and Kareem, A., 2009, "Gust-Front Factor: New Framework for Wind Load Effects on Structures," J. Struct. Eng.-ASCE, **135**(6), pp. 717–732.
[27] Kwon, D. K., Kareem, A., and Butler, K., 2012, "Gust-Front Loading Effects on Wind Turbine Tower Systems," J. Wind Eng. Ind. Aerodyn., **104–106**, pp. 109–115.
[28] Vakakis, A. F., Gendelman, O. V., Bergman, L. A., McFarland, D. M., Kerschen, G., and Lee, Y. S., 2009, *Nonlinear Targeted Energy Transfer in Mechanical and Structural Systems*, Springer Science+Business Media, B.V., Dordrecht, NL.
[29] Cveticanin, L., and Maretic, R., 1994, "A Van Der Pol Absorber for Rotor Vibrations," J. Sound Vib., **173**(2), pp. 145–155.
[30] Fujita, T. T., 1985, *The Downburst: Microburst and Macroburst*, University of Chicago, Chicago, IL.
[31] Fujita, T. T., 1986, *DFW Microburst on August 2, 1985*, University of Chicago, Chicago, IL.
[32] Wilson, J. W., Roberts, R. D., Kessinger, C., and McCarthy, J., 1984, "Microburst Wind Structures and Evaluation of Doppler Radar for Airport Wind Shear Detection," J. Appl. Meteorol. Climatol., **23**(6), pp. 898–915.
[33] Hjelmfelt, M. R., 1988, "Structure and Life Cycle of Microburst Outflows Observed in Colorado," J. Appl. Meteorol. Climatol., **27**(8), pp. 900–927.
[34] Oseguera, R. M., and Bowles, R. L., 1988, "A Simple, Analytic 3-D Downburst Model Based on Boundary Layer Stagnation Flow," National Aeronautics and Space Administration, Washington, DC, Report No. NASA-TM-100632.
[35] Solari, G., 2015, "Characteristics of Thunderstorms Relevant to the Wind Loading of Structures," Wind Struct., **20**(6), pp. 763–791.
[36] Burlando, M., Romanić, D., Solari, G., Hangan, H., and Zhang, S., 2017, "Field Data Analysis and Weather Scenario of a Downburst Event in Livorno, Italy, on 1 October 2012," Mon. Weather Rev., **145**, pp. 3507–3527.
[37] Romanić, D., Nicolini, E., Hangan, H., Burlando, M., and Solari, G., 2020, "A Novel Approach to Scaling Experimentally Produced Downburst-Like Impinging Jet Outflows," J. Wind Eng. Ind. Aerodyn., **196**, p. 104025.
[38] Jubayer, C., Elatar, A., and Hangan, H., 2016, "Pressure Distributions on a Low-Rise Building in a Laboratory Simulated Downburst," Proceedings of 8th International Colloquium on Bluff Body Aerodynamics and Applications (BBAA VIII), Boston, MA, June 7–11.
[39] Hangan, H., Romanić, D., and Jubayer, C., 2019, "Three-Dimensional, Non-Stationary and Non-Gaussian (3D-NS-NG) Wind Fields and Their Implications to Wind-Structure Interaction Problems," J. Fluids Struct., **91**, p. 102583.
[40] Chay, M. T., Albermani, F., and Wilson, R., 2006, "Numerical and Analytical Simulation of Downburst Wind Loads," Eng. Struct., **28**(2), pp. 240–254.
[41] Le, T.-H. L., and Caracoglia, L., 2017, "Computer-Based Model for the Transient Dynamics of a Tall Building During Digitally Simulated Andrews AFB Thunderstorm," Comput. Struct., **193**, pp. 44–72.
[42] Chen, X., 2008, "Analysis of Alongwind Tall Building Response to Transient Nonstationary Winds," J. Struct. Eng.-ASCE, **134**(5), pp. 782–791.
[43] Caracoglia, L., 2018, "Unified Stochastic Dynamic and Damage Cost Model for the Structural Analysis of Tall Buildings in Thunderstorm-Like Winds," ASCE-ASME J. Risk Uncertainty Eng. Syst. Part A: Civ. Eng., **4**(4), p. 04018043.
[44] Reed, D. A., and Scanlan, R. H., 1984, "Autoregressive Representation of Longitudinal, Lateral, and Vertical Turbulence Spectra," J. Wind Eng. Ind. Aerodyn., **17**(2), pp. 199–214.
[45] Bartoli, G., and Spinelli, P., 1993, "The Stochastic Differential Calculus for the Determination of Structural Response Under Wind," J. Wind Eng. Ind. Aerodyn., **48**(2–3), pp. 175–188.
[46] Bisplinghoff, R. L., Ashley, H., and Halfman, R. L., 1955, *Aeroelasticity*, Dover Publications Inc., Mineola, NY.
[47] Wagner, H., 1925, "Über Die Entstehung Des Dynamischen Auftriebes Von Tragflügeln (in German)," ZAMM - Z. Für Angew. Math. Mech., **5**, pp. 17–35.
[48] Jones, R. T., 1939, *The Unsteady Lift of a Finite Wing* (Technical Note 682), National Advisory Committee for Aeronautics, Washington, DC.
[49] Argentina, M., and Mahadevan, L., 2005, "Fluid-Flow-Induced Flutter of a Flag," Proc. Natl. Acad. Sci., **102**(6), pp. 1829–1834.
[50] Lin, Y.-K., and Cai, G.-Q., 1995, *Probabilistic Structural Dynamics*, McGraw-Hill, New York.
[51] Kloeden, P. E., Platen, E., and Schurz, H., 1994, *Numerical Solution of Stochastic Differential Equations Through Computer Experiments*, Springer-Verlag, Berlin-Heidelberg, Germany.
[52] Itô, K., 1951, *On Stochastic Differential Equations* (Vol. 4 of Memoirs of the American Mathematical Society), American Mathematical Society, Providence, Rhode Island.
[53] Wong, E., and Zakai, M., 1965, "On the Relation Between Ordinary and Stochastic Differential Equations," Int. J. Eng. Sci., **3**(2), pp. 213–229.
[54] Xie, W.-C., 2006, *Dynamic Stability of Structures*, Cambridge University Press, New York.
[55] Náprstek, J., 2001, "Stability Domains of Wind-Excited Random Nonlinear Systems Through Lyapunov Function," J. Wind Eng. Ind. Aerodyn., **89**(14–15), pp. 1499–1512.
[56] Pospíšil, S., Náprstek, J., and Hračov, S., 2006, "Stability Domains in Flow-Structure Interaction and Influence of Random Noises," J. Wind Eng. Ind. Aerodyn., **94**(11), pp. 883–893.
[57] Náprstek, J., and Pospíšil, S., 2012, "Response Types and General Stability Conditions of Linear Aeroelastic System With Two Degrees-of-Freedom," J. Wind Eng. Ind. Aerodyn., **111**, pp. 1–13.
[58] Náprstek, J., Pospíšil, S., and Yau, J.-D., 2015, "Stability of Two-Degree-of-Freedom Aeroelastic Models With Frequency and Time Variable Parametric Self-Induced Forces," J. Fluids Struct., **57**, pp. 91–107.
[59] Davenport, A. G., 1964, "Note on the Distribution of the Largest Value of a Random Function With Application to Gust Loading," Proc. Inst. Civ. Eng., **28**(2), pp. 187–196.
[60] Chen, X., 2014, "Extreme Value Distribution and Peak Factor of Crosswind Response of Flexible Structures With Nonlinear Aeroelastic Effect," J. Struct. Eng.-ASCE, **140**(12), p. 04014091.
[61] Roncallo, L., and Tubino, F., 2023, "Thunderstorm Gust Response Factor: A Closed-Form Solution," J. Wind Eng. Ind. Aerodyn., **240**, p. 105487.
[62] El-Hami, M., Glynne-Jones, P., White, N., Hill, M., Beeby, S., James, E., Brown, A., and Ross, J., 2001, "Design and Fabrication of a New Vibration-Based Electromechanical Power Generator," Sens. Actuators, A, **92**(1), pp. 335–342.

[63] Beeby, S., Wang, L., Zhu, D., Weddell, A., Merrett, G., Stark, B., Szarka, G., and Al-Hashimi, B., 2013, "A Comparison of Power Output From Linear and Nonlinear Kinetic Energy Harvesters Using Real Vibration Data," Smart Mater. Struct., **22**(7), p. 075022.
[64] Dompierre, A., Vengallatore, S., and Fréchette, L. G., 2019, "Achieving High Quality Factor Without Vacuum Packaging by High Density Proof Mass Integration in Vibration Energy Harvesters," J. Microelectromech. Syst.-IEEE, **28**(3), pp. 558–568.
[65] Jacobsen, L. S., 1930, "Steady Forced Vibration as Influenced by Damping: An Approximate Solution of the Steady Forced Vibration of a System of One Degree of Freedom Under the Influence of Various Types of Damping," ASME Trans. Am. Soc. Mech. Eng., **52**(2), pp. 169–178.
[66] van Kuik, G. A., 2007, "The Lanchester-Betz-Joukowsky Limit," Wind Energy, **10**(3), pp. 289–291.
[67] Dunn, P., and Dugundji, J., 1992, "Nonlinear Stall Flutter and Divergence Analysis of Cantilevered Graphite/Epoxy Wings," AIAA J., **30**(1), pp. 153–162.